JOURNAL OF SOLID STATE CHEMISTRY 100, 212–219 (1992)

HREM Studies of Phases Based on α-U_3O_8-Type Layers in the Cu_2O–Ta_2O_5 System

LENA JAHNBERG AND MARGARETA SUNDBERG

Department of Inorganic Chemistry, Arrhenius Laboratory, Stockholm University, S-10691 Stockholm, Sweden

Received November 26, 1991; in revised form March 2, 1992; accepted March 3, 1992

The high-resolution electron microscopy (HREM) technique was used to characterize phases in the Cu_2O–Ta_2O_5 system. The structures are closely related. They contain edge-sharing pentagonal TaO_7 bipyramids, forming layers of α-U_3O_8 type. These layers are either single or double, the latter linked by apex oxygens. The layers are interleaved by octahedral Ta sites and linearly coordinated Cu positions so that a three-dimensional network is formed. The symmetry is hexagonal (or trigonal). Varying sequences of single (S) and double (D) layers give different c-axis lengths. The phases $Cu_5Ta_{11}O_{30}$ and $Cu_3Ta_7O_{19}$ are well ordered, with SDSD and DD sequences, respectively. Other ordered sequences, (SS) in "$Cu_2Ta_4O_{11}$" and (SDSSDS) in "$Cu_7Ta_{15}O_{41}$," were also observed. Defects and disorder sometimes occur.

Introduction

In the system Cu_2O–Ta_2O_5 some phases have been observed which are structurally closely related to each other (*1*) and to the $Cu_5Ta_{11}O_{30}$ structure (*2*). They have similar unit cells with $a = b \approx 6.23$ Å (hexagonal axes) but different c-axis lengths. The structures may be expected to be built up of layers of edge-sharing pentagonal TaO_7 bipyramids (α-U_3O_8 type), single or double (sharing apex oxygens), connected by TaO_6 octahedra and linearly coordinated Cu, as determined from single-crystal X-ray data for the $Cu_5Ta_{11}O_{30}$ phase (*2*). The length of the c-axis thus depends on the numbers of single and double layers (*3*). Figure 1 shows the layer types and layer sequences observed in the $Cu_5Ta_{11}O_{30}$ structure and suggested for $Cu_3Ta_7O_{19}$ by the length of the c-axis.

Since the compositions of the two phases are very close to each other (68.75 and 70.00 mol% Ta_2O_5), small variations in sample composition may be expected to reflect layer sequence irregularities, such as were often indicated by diffuse powder patterns. A high-resolution electron microscopy (HREM) investigation was started in order to verify the previously suggested ordered structure models, but also at the atomic level to elucidate the presence of order, disorder, and intergrowth between the various structures formed. Some preliminary results are presented below.

Experimental

The samples were prepared from mixtures of Cu_2O and Ta_2O_5 in evacuated silica tubes and were characterized by Guinier powder diffraction (*1*). In this study all syn-

0022-4596/92 $5.00

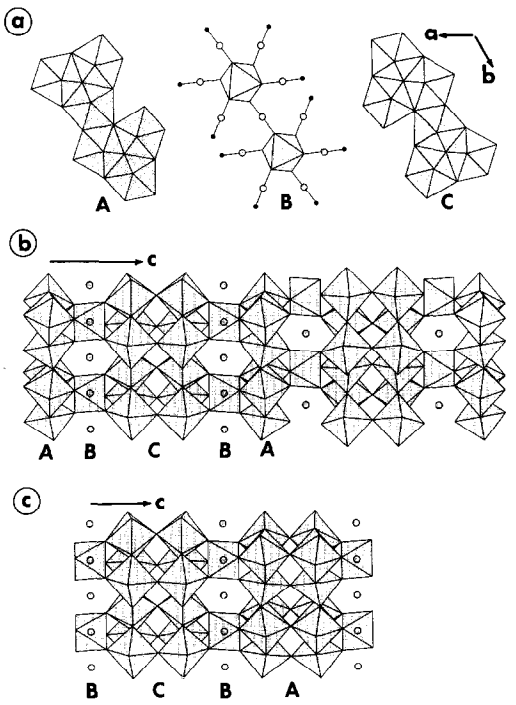

FIG. 1. (a) The layers of polyhedra projected along the c-axis. A and C: Edge-sharing pentagonal TaO_7 bipyramids yielding layer composition Ta_3O_8. B: TaO_6 octahedra and linear CuO_2 yielding layer composition A_3TaO_3; with A = Cu, the sites are not always fully occupied. Black dots are oxygens in adjacent octahedra. (b) The structure of $Cu_5Ta_{11}O_{30}$ viewed along the a-axis. (c) The structure model of $Cu_3Ta_7O_{19}$ projected along [100].

theses were made in the temperature range 1000–1100°C.

The electron microscope specimens were prepared in the following way: a small amount of the sample was crushed in an agate mortar and dispersed in n-butanol. A few drops of the resultant suspension were put on a holey carbon film supported on a Cu grid and were left to dry. The grids were then examined in a JEOL 200CX electron microscope equipped with a double-tilt lift goniometer stage and operated at an accelerating voltage of 200kV. The HREM images were recorded with an objective aperture corresponding to approximately 0.41 $Å^{-1}$ in reciprocal space. Simulated images were calculated with a slightly modified local version of the SHRLI-suite of programs (*4*).

Results and Discussion

Electron microscopy studies of the $Cu_5Ta_{11}O_{30}$ phase showed that most of the crystal fragments tended to orient themselves with the c-axis (c = 32.550 Å) parallel to the electron beam. Figure 2a (top) illustrates the corresponding HREM image. However, a micrograph in this projection will not contain any direct information on stacking sequences or defects along the c-axis. Such information will instead be obtained from HREM images recorded along [100] or some other [hk0] direction of the orthohexagonal cell with $a \approx 6.23$ Å and $b \approx 10.79$ Å, i.e., perpendicular to the direction of varying layer sequences. Figure 2b shows an HREM image of a thin crystal fragment aligned with $[100]_{orth.}$ parallel to the electron beam. The contrast in the micrograph can be described as an ordered arrangement of double and single black lines parallel to the [010] direction. Simulated images of the $Cu_5Ta_{11}O_{30}$ structure were calculated using the atomic parameters from the single-crystal X-ray investigation (*2*). However, the coordinates were first transformed to the orthohexagonal cell given above. Figure 2c shows the projected electron density of $Cu_5Ta_{11}O_{30}$ along $[100]_{orth.}$ with an overlay of the corresponding structure model. In the micrograph the layers of seven-coordinated tantalum atoms all appear as unresolved black lines, whereas the octahedrally coordinated Ta atoms are seen as black dots. A set of calculated images projected along [100] is shown in Fig. 2d, and a calculated image ([001] zone) is inserted in Fig. 2a (bottom). There is good agreement between the contrast features in the HREM images and the calculated images. The typical sequence for the $Cu_5Ta_{11}O_{30}$ structure (Fig. 2c) is single

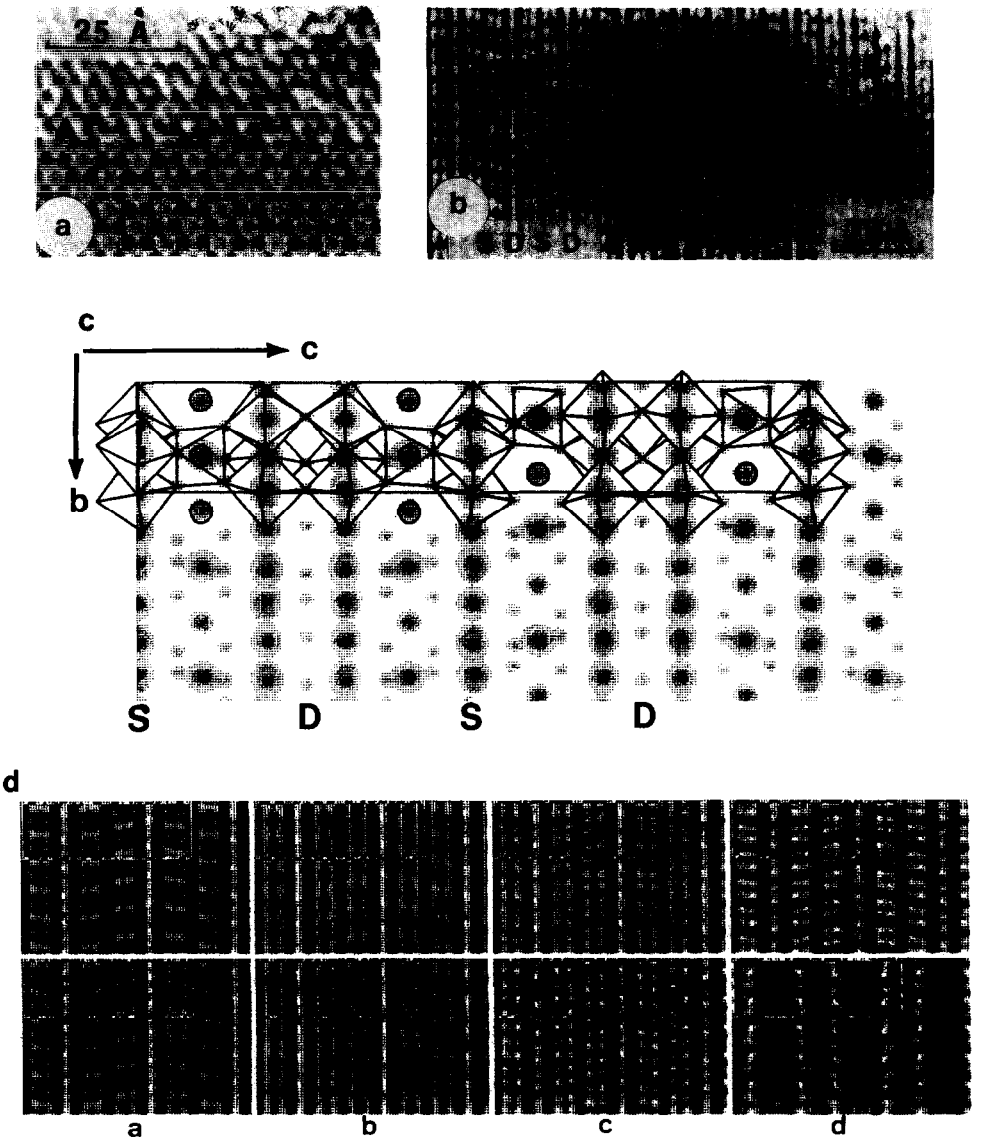

FIG. 2. (a) HREM image of the $Cu_5Ta_{11}O_{30}$ phase along [001], with a simulated image inserted: crystal thickness 32.6 Å, defocus value: −1100 Å. (b) HREM image of $Cu_5Ta_{11}O_{30}$, [100] zone. (c) Electron density projection along [100] with an overlay of the structure model in Fig. 1b. S = single pentagonal TaO_7 bipyramid layer, D = double pentagonal TaO_7 bipyramid layer. (d) Simulated images along [100], crystal thickness 18.7 Å (top), 39.4 Å (bottom). Defocus values (a–d): −400–−700 Å in steps of −100 Å.

layer of pentagonal TaO_7 bipyramids (S), layer of octahedra, double layer of pentagonal TaO_7 bipyramids (D), layer of octahedra. Thus, the structure is characterized by the stacking sequence SD, with SDSD making up one unit cell width in the *c*-axis direction, as can be distinguished in Fig. 2b.

We have not yet been able to prepare any single-phase $Cu_3Ta_7O_{19}$ samples with our method. The Guinier powder pattern of the

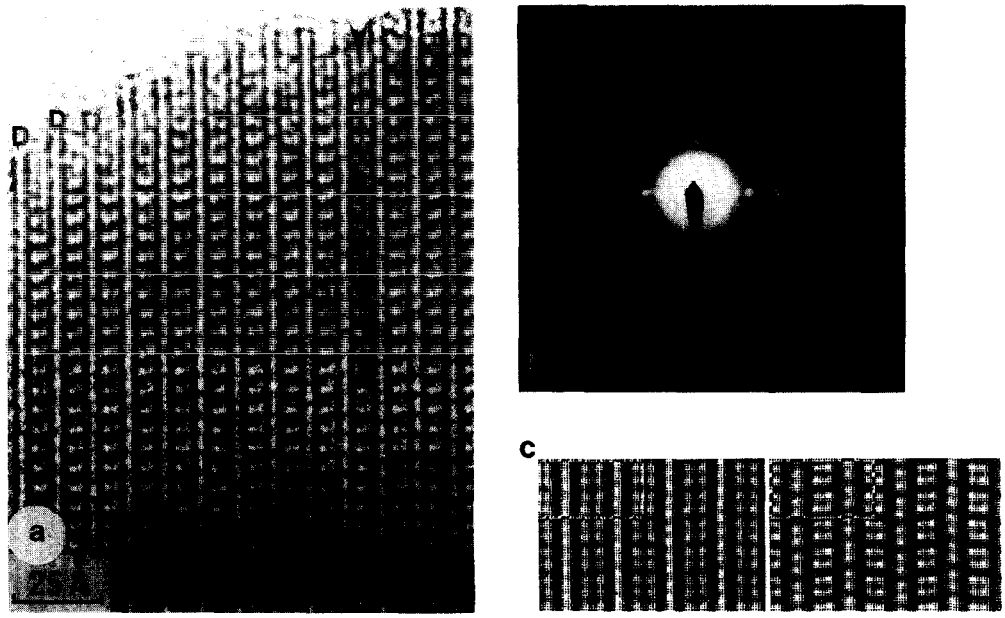

FIG. 3. (a) HREM image of $Cu_3Ta_7O_{19}$ ([100] projection) with a defect marked by arrows. (b) The corresponding electron diffraction pattern. (c) Simulated images of the model in Fig. 1c: crystal thickness 18.7 Å, defocus values −600 Å (left) and −700 Å (right).

sample used in this study showed the presence of $Cu_5Ta_{11}O_{30}$, $Cu_3Ta_7O_{19}$, and an L-Ta_2O_5-type phase. The HREM image in Fig. 3a was obtained from a thin crystal fragment believed to represent the $Cu_3Ta_7O_{19}$ phase, as $c \approx 19.9$ Å from the corresponding electron diffraction pattern (Fig. 3b). The micrograph shows an ordered region with pairs (doublets) of black lines separated by dotted lines. The suggested structure of $Cu_3Ta_7O_{19}$ in Fig. 1c contains only double layers of TaO_7 bipyramids alternating with octahedrally coordinated Ta and linearly coordinated Cu. Simulated images of this structure model (Table I) were calculated. There is good agreement between the observed image, at the thin crystal edge in Fig. 3a, and the calculated one to the left in Fig. 3c, which verifies the suggested structure model. Typical for the $Cu_3Ta_7O_{19}$ structure is the stacking of only D layers, with DD representing one unit cell width. One type of structural defect observed in the examined crystals can be seen in Fig. 3a. The black contrast features (marked by arrows) indicate that some other type of atom arrangement is present in a layer consisting of octahedrally coordinated Ta atoms and linearly coordinated Cu atoms.

TABLE I

ATOMIC PARAMETERS OF THE $Cu_3Ta_7O_{19}$ MODEL

Atom	x	y	z
Ta(1)	0	0	0
Ta(2)	0.69	0.03	0.156
Cu	$\frac{1}{2}$	0	0
O(1)	0.76	0.03	0.057
O(2)	$\frac{2}{3}$	$\frac{1}{3}$	0.140
O(3)	0.34	0.92	0.156
O(4)	0	0	0.164
O(5)	0.70	0.06	$\frac{1}{4}$

Note. Space group $P6_3/m$; cell parameters a = 6.2323 Å and c = 20.156 Å.

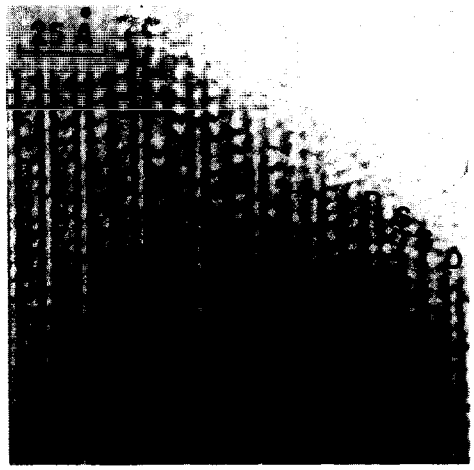

FIG. 4. HREM image ([100] projection) showing a disordered region.

Figure 4 shows an HREM image of a different part of the same crystal fragment as in Fig. 3. The micrograph illustrates an intergrowth of the $Cu_3Ta_7O_{19}$ and $Cu_5Ta_{11}O_{30}$ structures. Doublets of black lines (D) representative of the $Cu_3Ta_7O_{19}$ phase are seen to the left, while an ordered arrangement of single and double black lines (SD), typical of the $Cu_5Ta_{11}O_{30}$ structure, can be distinguished in the middle of Fig. 4. A new type of stacking sequence (SSD), corresponding to two single and one double layer, can also be discerned to the right in Fig. 4.

A $Cu_2Ta_4O_{11}$ phase, with only single TaO_7 bipyramid layers as in the $CaTa_4O_{11}$ (*5*) and $Na_2Ta_4O_{11}$ (*6*) phases, is normally not formed at the stoichiometric composition. However, it was observed occasionally together with other phases. The powder patterns showed that the copper and sodium compounds had closely similar trigonal (rhomboedral) unit cells and thus the same tantalum–oxygen framework. The electron diffraction pattern (Fig. 5a) of the $Cu_2Ta_4O_{11}$ phase showed the typical monoclinic appearance of this type of cell viewed along $[100]_{trig}$. The connection between these trigonal and monoclinic cells has been discussed in Ref. (*7*). The micrograph in Fig. 5b shows an ordered region with single black lines. In analogy with the $Cu_5Ta_{11}O_{30}$ structure, these black lines were interpreted as corresponding to single (S) layers separated by TaO_6 octahedra and Cu atoms. The structure model is illustrated in Fig. 5c and shows a characteristic stacking sequence of S. Simulated images of the structure (Table II) confirmed the interpretation of the HREM image. There is good agreement between the recorded image of the thinner part of the crystal in Fig. 5b and the calculated image (Fig. 5d). The stoichiometry of $Cu_2Ta_4O_{11}$ allows only 2/3 of the Cu positions to be occupied. The $Cu_2Ta_4O_{11}$ phase can be stabilized by the increase in Cu content concomitant with substituting some Zr for Ta.

Figure 6 shows another occasionally occurring ordered phase. The length of the *c*-axis indicates that the structure should contain four S and two D layers. However, the stacking sequence could only be determined from the HREM images. The micrographs in Fig. 6a and Fig. 6b ([010] and [100] projections, respectively) clearly show an ordered arrangement of two single black lines and one doublet of black lines. In analogy with the results obtained above, this was interpreted as shown in the structure model (Fig. 6c). A set of simulated images was calculated from the atomic coordinates given in Table III. There is good agreement between the observed (Fig. 6b) and calculated images. The structure can be described as two S layers followed by one D layer (SSD). The composition of the structure corresponds to $Cu_7Ta_{15}O_{41}$ and the layer sequence SDSSDS represents one unit-cell width. The stacking sequence SSD was also observed as a defect in the right-hand part of Fig. 4. Like the single-layer phase, $Cu_2Ta_4O_{11}$, this phase has not been reproducibly obtained so far, and it does not form at the stoichiometric composition. The Cu_7

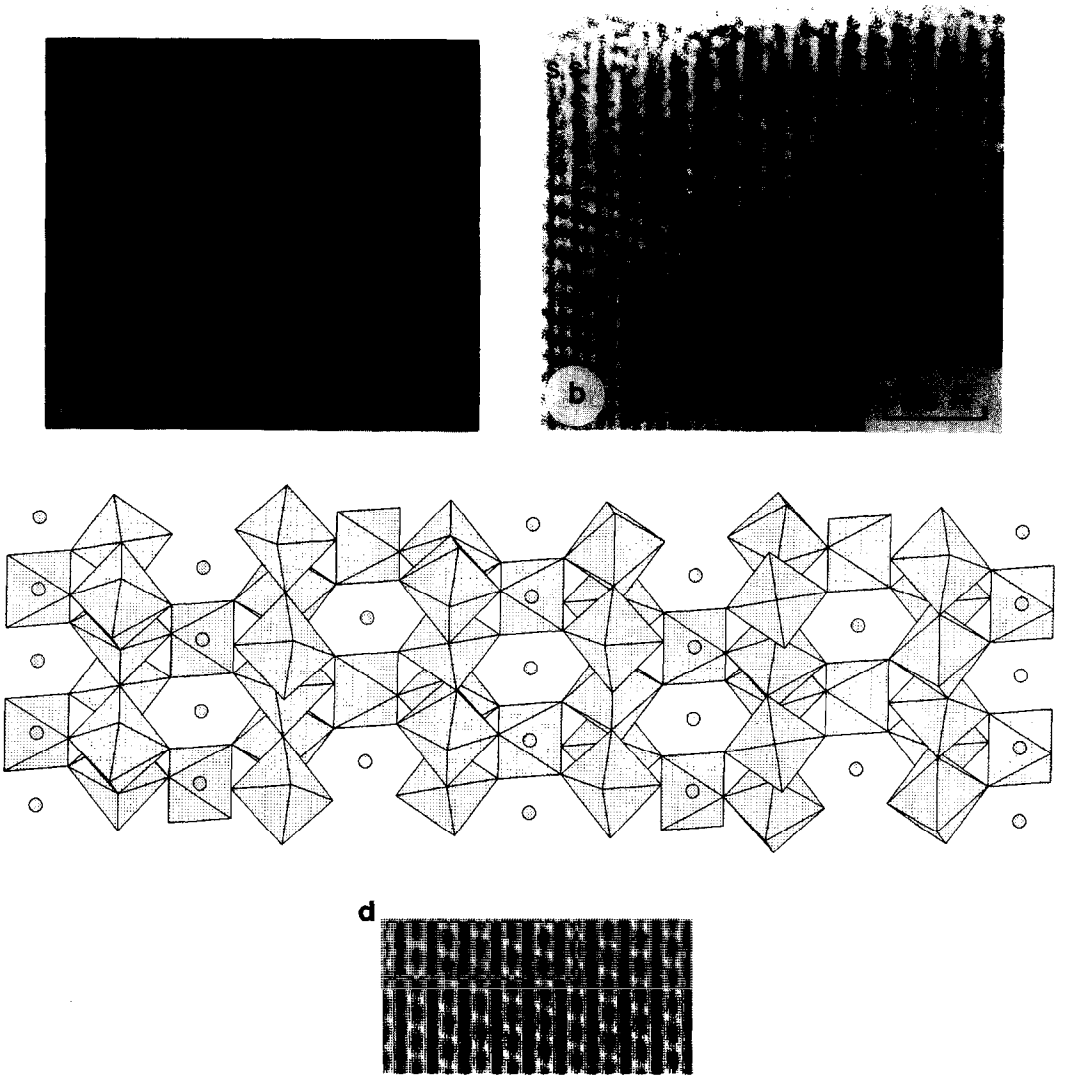

FIG. 5. (a) Electron diffraction pattern of "$Cu_2Ta_4O_{11}$," [100] zone. (b) The corresponding HREM image. (c) Structure model of $Cu_2Ta_4O_{11}$. (d) Calculated image: crystal thickness ≈19 Å, defocus value −500 Å.

$Ta_{15}O_{41}$ structure can be described as twinning of slabs of the S-layer phase, where the twin plane corresponds to the plane of interleaving apex oxygen atoms in the double layer. With a similar description of the $Cu_5Ta_{11}O_{30}$ and $Cu_3Ta_7O_{19}$ structures, the spacing between the twin planes decreases with decreasing Cu_2O content.

Two electron microscopy investigations have previously been published on the related structures $CaTa_4O_{11}$ (*8*) and $LaTa_7O_{19}$ (*9*). These structures were only examined with the [001] direction parallel to the electron beam, however, which means that no direct information on the stacking sequences perpendicular to the *c*-axis could

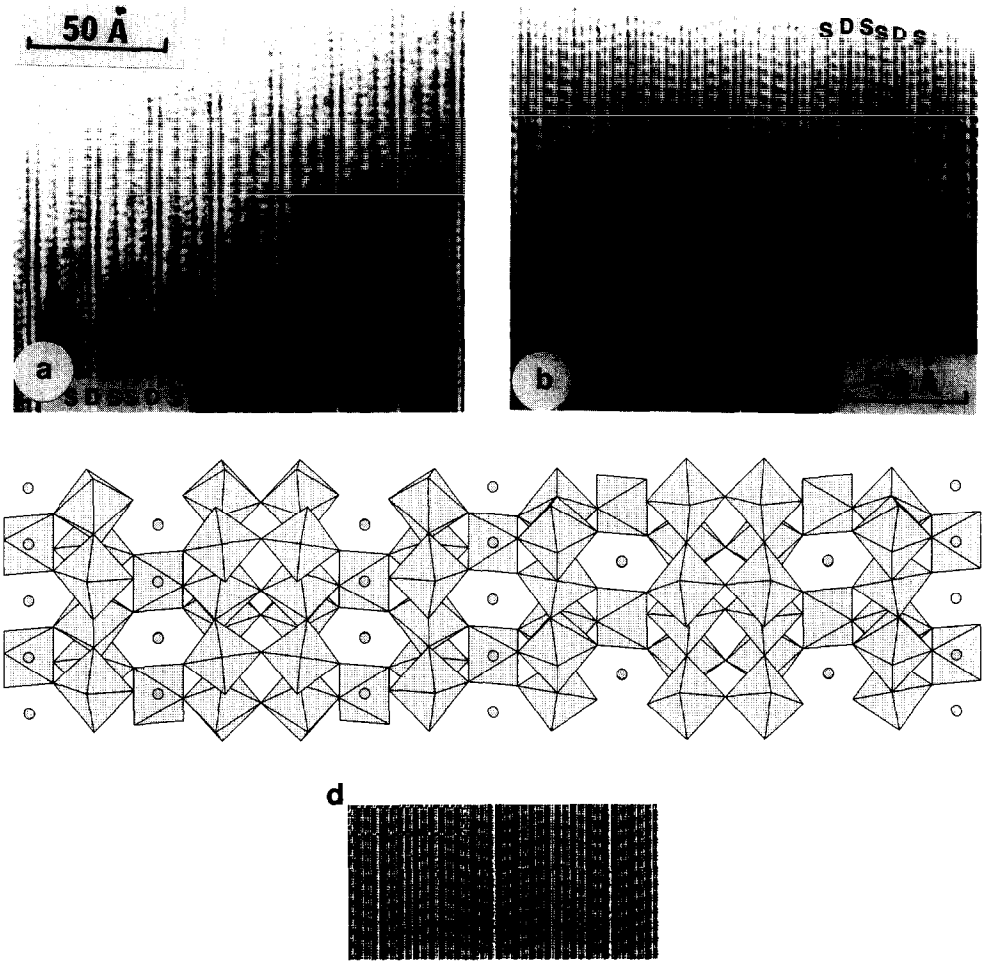

FIG. 6. HREM images of ordered regions of the "$Cu_7Ta_{15}O_{41}$" phase: (a) [010] projection, (b) [100] projection. (c) Structure model of $Cu_7Ta_{15}O_{41}$ in [100] projection. (d) Simulated image of the model in Fig. 6c. Crystal thickness 18.7 Å, defocus value −500 Å.

be obtained. In the present study theoretical image calculations of the Cu phases along the [001] direction clearly showed that it was not possible to distinguish between the closely related structures in this projection. However, the HREM results presented above along the [100] direction confirm that the ordered phases are built up of different combinations of single and double layers of pentagonal TaO_7 bipyramids, and they also reveal occasionally occurring defects as deviating stacking arrangements.

Several structures with single or double pentagonal-bipyramid layers have been reported earlier and have been summarized as a family of related structures with the general formula $A_xM_{3n+1}O_{8n+3}$ (M = Nb or Ta) with $n = 1$ for single layers and $n = 2$ for double layers. Layers of pentagonal MO_7 bipyramids have the composition M_3O_8, and layers of octahedra A_xMO_3

TABLE II

ATOMIC PARAMETERS OF THE $Cu_2Ta_4O_{11}$ MODEL

Atom	x	y	z
Ta(1)	0	0	0
Ta(2)	0.36	0	$\frac{1}{4}$
Cu[a]	$\frac{1}{2}$	0	0
O(1)	0	0	0.092
O(2)	0.75	0	$\frac{1}{4}$
O(3)	0.43	0.06	0.302

Note. Space group $R\bar{3}c$; cell parameters $a \approx 6.23$ Å and $c \approx 37.34$ Å.

[a] $\frac{2}{3}$ occupancy.

(*3*). The phases studied in this work are combinations of $n = 1$ and $n = 2$. For full occupancy of the linearly coordinated Cu(I) position the value of x is 3 (compare Fig. 1a). In $Cu_3Ta_7O_{19}$ this high value is reached, but for $Cu_5Ta_{11}O_{30}$ the occupancy is 5/6, for $Cu_7Ta_{15}O_{41}$, 7/9, and for $Cu_2Ta_4O_{11}$, only 2/3. Vacancies at the Cu positions are thus necessary for forming different sequences of S and D.

TABLE III

ATOMIC PARAMETERS OF THE $Cu_7Ta_{15}O_{41}$ MODEL

Atom	x	y	z
Ta(1)	0	0	0
Ta(2)	0.70	0.03	0.069
Ta(3)	$\frac{2}{3}$	$\frac{1}{3}$	0.139
Ta(4)	0.36	0	0.208
Cu(1)[a]	$\frac{1}{2}$	0	0
Cu(2)[a]	0.67	0.84	0.139
O(1)	0.77	0.04	0.026
O(2)	$\frac{2}{3}$	$\frac{1}{3}$	0.062
O(3)	0.58	0.67	0.069
O(4)	0	0	0.076
O(5)	0.70	0.09	0.112
O(6)	0.43	0.06	0.166
O(7)	$\frac{1}{3}$	$\frac{2}{3}$	0.201
O(8)	0.75	0	0.208
O(9)	$\frac{2}{3}$	$\frac{1}{3}$	0.212
O(10)	0.37	0.96	$\frac{1}{4}$

Note. Space group $P6_3/m$; cell parameters $a = 6.2262$ Å and $c = 44.877$ Å.

[a] 7/9 occupancy.

The fact that different sequences occur in the same crystal explains the difficulty met in getting single-phase samples, and it also shows why the powder patterns are often diffuse at the stoichiometric composition. So far, $Cu_5Ta_{11}O_{30}$ with some Cu vacancies seems to be stable, but very careful control of the formation conditions is necessary to establish if a phase is stable or metastable.

There are several compounds ATa_7O_{19}, where A is eight-coordinated in a fully occupied position, e.g., A = La–Nd (*9–11*) and Bi (*12*). For a corresponding single-layer structure the composition should be $A_{2/3}Ta_4O_{11}$, where the eight-coordinated position would be only 2/3 occupied. If an incomplete occupancy is possible, phases similar to those in the Cu_2O–Ta_2O_5 system, with both S and D layers, might form.

Acknowledgment

This investigation was financially supported by the Swedish Natural Science Research Council.

References

1. L. JAHNBERG, *Acta Chem. Scand. Ser. A* **41,** 527 (1987).
2. L. JAHNBERG, *J. Solid State Chem.* **41,** 286 (1982).
3. L. JAHNBERG, *Mater. Res. Bull.* **16,** 513 (1981).
4. M. O'KEEFE, P. R. BUSECK, AND S. IIJIMA, *Nature (London)* **274,** 322 (1978).
5. L. JAHNBERG, *J. Solid State Chem.* **1,** 454 (1970).
6. R. MATTES AND J. SCHAPER, *Rev. Chim. Mine.* **22,** 817 (1985).
7. L. JAHNBERG, *Chem. Commun. Univ. Stockholm* **XIII** (1971).
8. B. LANGENBACH-KUTTERT, W. MERTIN, AND R. GRUEHN, *Z. Naturforsch.* **40b,** 1651 (1985).
9. B. LANGENBACH-KUTTERT, J. STURM, AND R. GRUEHN, *Z. Anorg. Allg. Chem.* **543,** 117 (1986).
10. B. M. GATEHOUSE, *J. Solid State Chem.* **27,** 209 (1979).
11. U. SCHAFFRATH AND R. GRUEHN, *Z. Anorg. Allg. Chem.* **588,** 43 (1990).
12. W. STEMMER AND R. GRUEHN, *Z. Anorg. Allg. Chem.* **581,** 183 (1990).